JOURNAL OF MATERIALS SCIENCE **33** (1998) 5339–5349

Single crystal fibers of yttria-stabilized cubic zirconia with ternary oxide additions

F. J. RITZERT, H. M. YUN, R.V. MINER
NASA Lewis Research Center, Cleveland, OH 44135-3191, USA

Single crystal fibers of yttria (Y_2O_3)-stabilized cubic zirconia (ZrO_2) with ternary oxide additions were grown using the laser float zone fiber processing technique. Ternary additions to the ZrO_2-Y_2O_3 binary system were studied aimed at increasing strength while maintaining the high coefficient of thermal expansion of the binary system. Statistical methods aided in identifying the most promising ternary oxide candidate (Ta_2O_5, Sc_2O_3, and HfO_2) and optimum composition. The yttria range investigated was 14 to 24 mol % and the ternary oxide component ranged from 1 to 5 mol %. Hafnium oxide was the most promising ternary oxide component based on 816 °C tensile strength results and ease of fabrication. The optimum composition for development was 81ZrO_2-14Y_2O_3-5HfO_2 based upon the same elevated temperature strength tests. Preliminary results indicate process improvements could improve the fiber performance. We also investigated the effect of crystal orientation on strength.

1. Introduction

Fiber reinforced metal and intermetallic composites (MMC and IMC) are candidate research materials to enable high performance advanced gas turbine engines. Single crystal oxide fiber reinforcements have the potential to possess the required high strength, thermal expansion coefficient (CTE), creep resistance and environmental durability [1]. The operating environment is characterized by high temperatures, steep thermal gradients, stresses unique to rotating components, both monotonic and cyclic thermomechanical loads, and environmental attack.

This work was intended to help identify a viable high expansion fiber to reinforce well-developed high-temperature matrices such as superalloys or the aluminides. The long range goal is to produce an MMC as a viable alternative to the current monolithic alloys in high-temperature engine service. Specific fiber strength goals were developed to exceed superalloy performance. Fibers were grown using the laser float zone apparatus (LFZ) [2].

The most studied single crystal fibers to date are the sapphire and alumina-YAG eutectic fibers from Saphikon [3] produced by the Edge-defined Film Growth (EFG) process. Efforts to develop single crystal sapphire reinforced MMCs have decreased due to issues related to both CTE mismatch and fiber degradation during fabrication and in simulated service [4]. A primary mechanism of fiber breakage is the poor match in thermal expansion between sapphire and potential metal matrices. Breakage occurs during cooling from the composite fabrication temperature and is aggravated by significant fiber strength degradation due to even minor chemical reactions with numerous matrices [4]. Also, sapphire fibers have been reported to be subject to slow, low temperature crack growth causing a low strength value ~0.6 GPa at 400 to 800 °C [5–7]. However Cr^+ doped yttrium-aluminum-garnet (YAG) were reported to retard the slow crack growth in the single crystal alumina [8].

Another candidate fiber, yttria-stabilized cubic zirconia (YSZ) in single crystal form may also have potential as a MMC reinforcement. YSZ possesses a high CTE of 13×10^{-6}/°C, fairly close to that of superalloys or aluminides (about 16×10^{-6}/°C), much higher than that of sapphire (about 8×10^{-6}/°C). Calculations show that this reduction in CTE mismatch will result in significant reductions in residual stresses. In comparison to the hexagonal sapphire, the YSZ possesses more isotropic properties because of its cubic crystal structure as well as a relatively high 3000 °C melt temperature (Fig. 1). In addition other properties such as modulus (~275 GPa) and density make this fiber a well-suited reinforcement. Single crystal YSZ fibers have also been shown to be chemically compatible with Ni- or Fe-base MMC matrix materials [9]. Further, the Y_2O_3-stabilized single crystal fibers were reported to have high strength and creep resistance up to 1400 °C in the range of 9 to 21 mol % Y_2O_3 regime [10–13]. Potential solid solution strengthening or precipitation hardening effects could cause a two- to four-fold increase in flow stress at high temperatures and result in excellent fracture toughness in the 9.4 to 21 mol % Y_2O_3 addition [10–13]. Based upon phase diagrams and physical properties, several oxides were included in the screening process with Y_2O_3 and X_aO_b levels not to exceed 20 and 10 mole %, respectively. X_aO_b (X = Cr, Ta, Ti, La, Hf, Ca, Al, Mg, Sc, Er, Yb) limits were imposed because of density considerations.

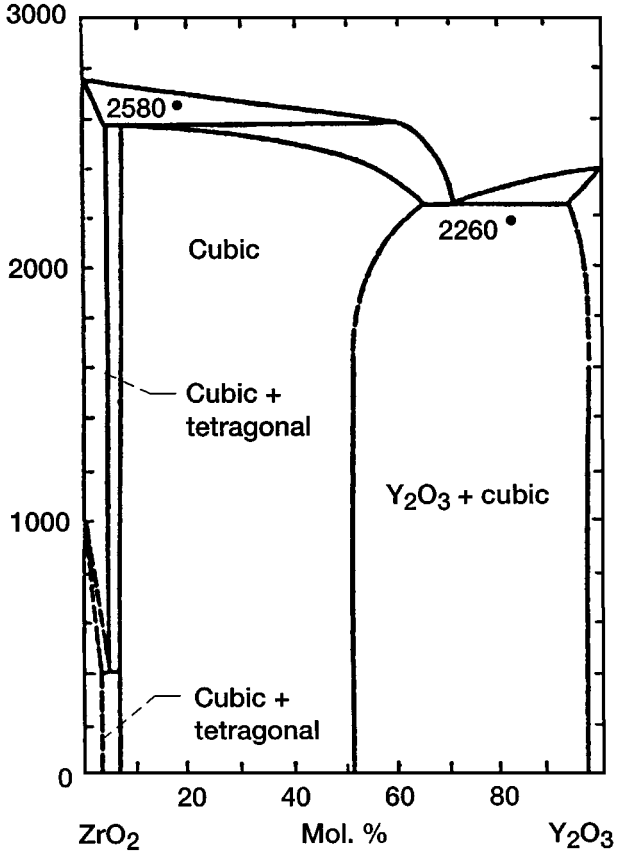

Figure 1 ZrO_2-Y_2O_3 phase diagram.

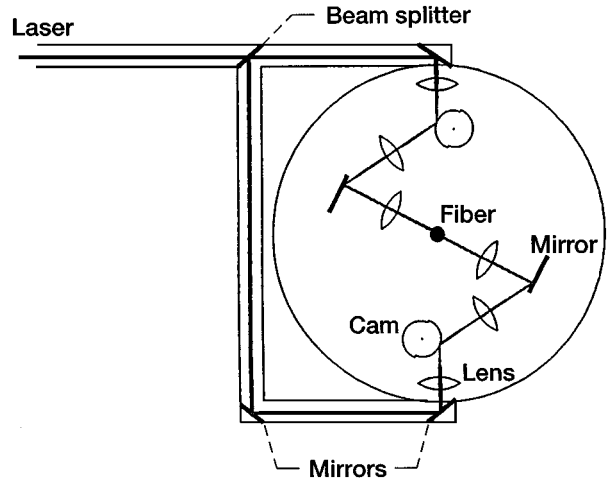

Figure 2 Schematic of laser path in the laser float zone system.

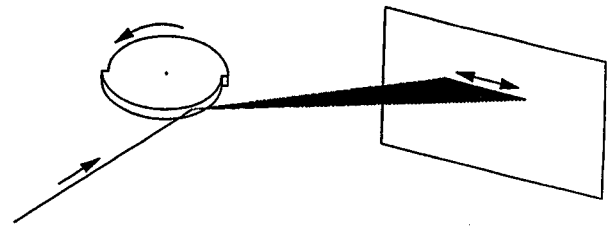

Figure 3 Schematic of linear laser line scan.

2. Materials and procedures

Ternary oxide additions were screened to combine with yttria-stabilized cubic zirconia to arrive at a promising ternary fiber composition (ZrO_2-Y_2O_3-X_aO_b) for MMC reinforcement. A manageable list of ternary oxides (X_aO_b) for investigation was selected based on several factors including the molecular weight, melting point, density, vapor pressure, phase diagram inspection, and molten zone stability during single crystal growth [14]. Levels of Y_2O_3 and X_aO_b were varied in an attempt to optimize fiber composition. A statistical methods approach was chosen as the most efficient method for determining an optimum zirconia-based fiber composition [15].

2.1. Material preparation and fiber growth

The laser float zone (LFZ) fiber growth apparatus used in this study [2] is capable of delivering 600 watts of CO_2 laser power needed for high-melting point materials and avoids the risk of contaminants inherent in crucible based methods. One laser beam is generated and then split. These two beams are then focused and directed perfectly towards each other at the center of the chamber (Fig. 2). These opposing beams are converted into linear laser scans as they impinge upon the rotating cam. The scan is the result of the increasing radius of the cam, the two steps, and its high frequency of rotations per second (Fig. 3). Fig. 4 shows how a floating zone is created in the system when a feedrod of specific composition is fed into opposing laser scans where it is melted and combined with a single crystal fiber seed. Fig. 5 represents the three primary components involved in LFZ crystal formation – the feedrod, the molten zone, and the solidified crystal.

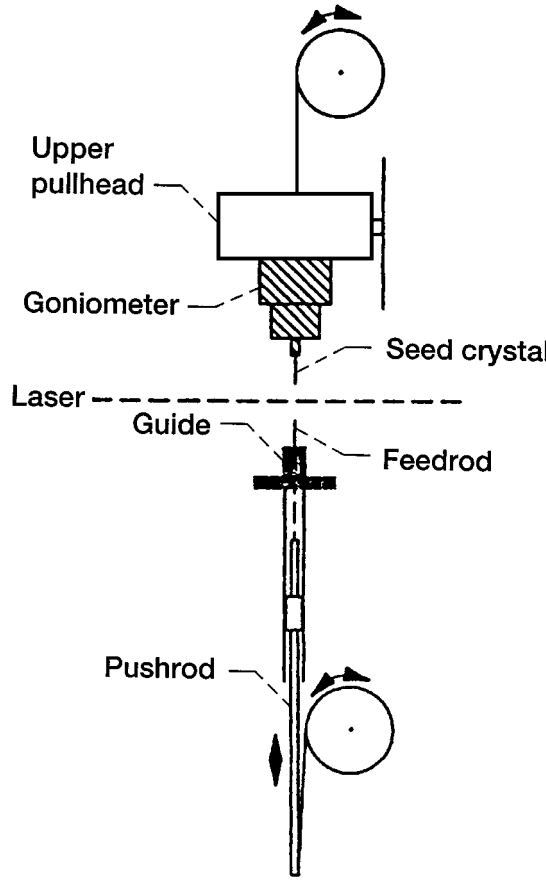

Figure 4 Schematic of laser float zone apparatus growth train.

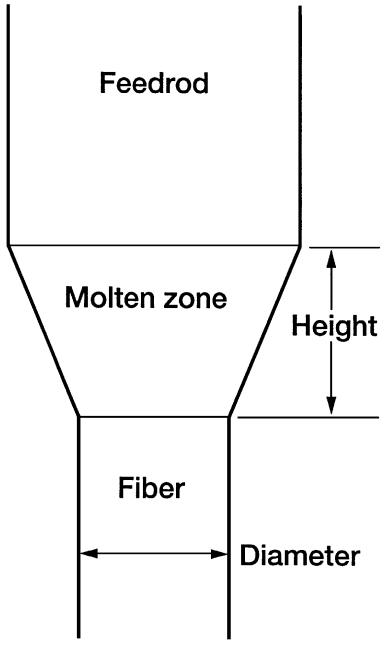

Figure 5 Components of laser float zone fiber growth.

Particular to this investigation, the ceramic feed rods were prepared from high purity fine oxide particles (<325 mesh) by a conventional slurry technique [16]. Feed rod diameter measured ∼635 μm. The fiber was passed two times through the laser floating zone while attenuating the diameter in ratios of 2 : 1 and 3 : 1 to achieve a final single crystal oxide fiber with a diameter of ∼175 μm. The fiber growth speeds were 200 to 300 mm/h. The laser floating zone apparatus was operated in dry air at temperatures from 2500 to 2900 °C. Ternary ZrO_2 fibers were pre-evaluated based on diameter uniformity and room temperature bend testing. A typical ZrO_2 fiber is shown in Fig. 6, as well as a commercial single crystal Al_2O_3 grown by EFG for comparison. Fibers which demonstrated good preliminary mechanical integrity were thoroughly tested.

The crystallographic orientations of selected fibers were determined using X-ray diffraction methods. Single crystal seeds were mounted on an adjustable crystal goniometer, which was mounted directly on the LFZ machine.

2.2. Fiber testing

Fiber strengths at 816 °C were measured using a micropulling machine modified to accommodate small diameter fibers [17] in addition to a conventional Instron testing frame for comparative purposes. The difference in the strength between these two types of machines was not significant, as the standard deviation was nearly the same. The specimen length for both cases was 75 mm, and was prepared using paper tabs, using ASTM Standard D3379-75 [18]. The furnace hot zone length was 25 mm and taken as the specimen gauge length. After reaching temperature, the specimen was held for 5 minutes at temperature before loading. The breaking load and individual fiber diameters (determined under a 200× split image microscope) were used to calculate the fiber strengths and subsequently studied by microstructural and X-ray analysis.

The elastic modulus was determined from the load vs. displacement curve using a known machine compliance [19] which compared favorably to the measurement using flexural resonance techniques [20]. In both cases it was assumed that the fiber diameter was uniform within the gauge length and that the machine compliance was constant, independent of load.

Fiber thermal expansion was also measured using a Mettler Dilatometer [21]. The ZrO_2 fiber (10 mm gauge length) was vertically held using a pre-calibrated specimen holder. The specimen was heated up to ∼800 °C at a constant heating rate of 10 °C/min and the displacement was measured by a Linear Variable Differential Transformer (LVDT). The temperature and displacement readings were used to calculate instantaneous thermal expansion coefficients.

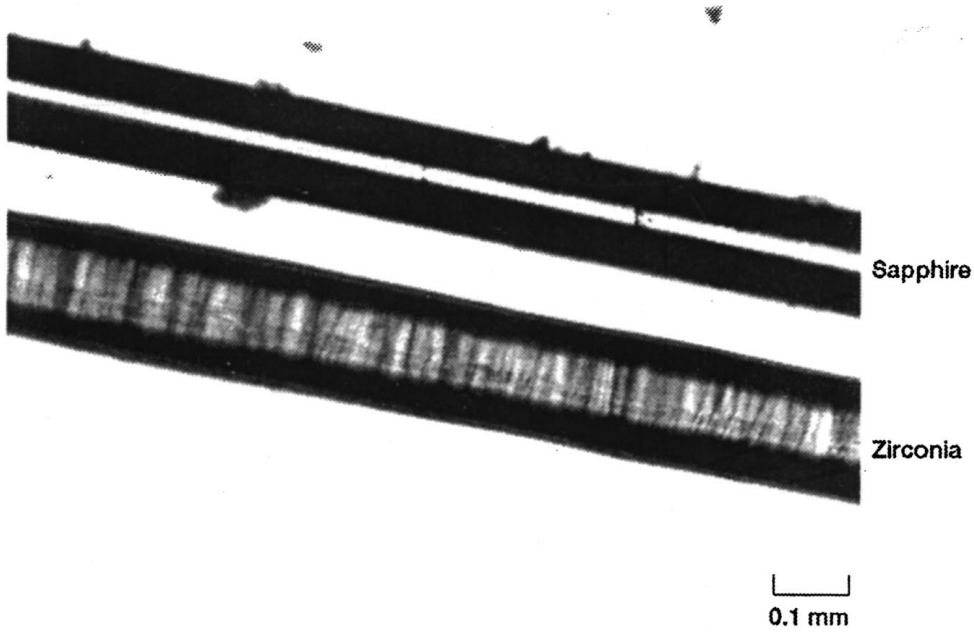

Figure 6 Surface finish of ZrO_2 LFZ fiber and Al_2O_3 Saphikon fiber.

3. Results and discussion

3.1. Strength goals

New candidate materials for high temperature applications must exceed conventional nickel-base superalloy performance in order to justify further development. Therefore superalloy properties serve as baseline information to compare new materials. The strength goal for single crystal YSZ fiber was calculated assuming an MMC with a nickel-base matrix and ideal interfacial conditions [22], using a two-component rule-of-mixtures for composite strength. For the required fiber strength two typical cases were analyzed, with a matrix strength contribution,

$$\sigma_f > (1/V_f)[(\rho_c/\rho_m)\sigma_m - V_m * \sigma_m] \quad (1)$$

and with no matrix strength contribution,

$$\sigma_f > (1/V_f)(\rho_c/\rho_m)\sigma \quad (2)$$

where σ and σ_m are monolithic superalloy and composite matrix strength respectively, ρ_c and ρ_m are composite and matrix density, V_f is fiber volume fraction, and σ_f is the minimum goal strength for fibers. Here it was assumed that (1) the ZrO_2 fibers did not degrade during composite consolidation, (2) the fibers possessed a high Weibull modulus neglecting a bundle factor that accounts for the statistical distribution of fiber strength in a composite [23], and (3) the matrix for the composite is Waspalloy. The fiber strength goal was set as the minimum strength required to achieve a MMC strength equal to that of a conventionally cast superalloy such as polycrystalline Mar-M200 or Alloy 713C. A modern single crystal nickel-base superalloy, like PWA1480, may have a similar high temperature fast fracture tensile strength compared to Mar-M 200 [24]. Fig. 7 displayed the required fiber tensile strength as a function of temperature to compare with the cast superalloys based upon Equations 1 and 2. A high fiber tensile strength is needed when the matrix does not share load. However, this is unrealistic since load sharing is intrinsic to composites [1]. The fiber tensile strength needed also increases with decreasing fiber volume fraction. In general, 30 to 50% fiber volume fraction is typical for unidirectional composites, and the load may be shared 50 to 70% by the matrix. The goal fiber strength had a maximum of ~0.8 GPa for composites with $V_f = 0.4$, from room temperature to 1200 °C. This was varied from ~0.7 to ~0.9 GPa for $V_f = 0.5$ and $V_f = 0.3$ composites, respectively. This indicates that newly developed ZrO_2 fiber reinforced composites would be superior in the longitudinal direction compared to a conventional superalloy when the ZrO_2 fiber strength at 816 °C is ~1 GPa.

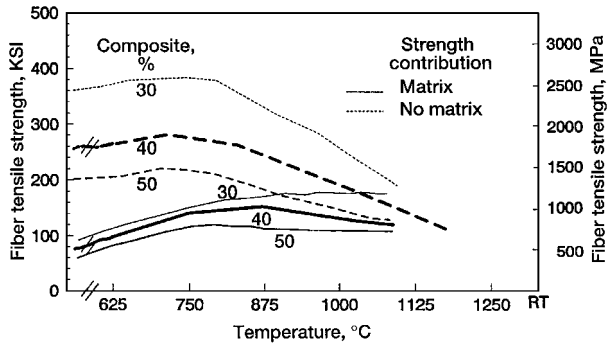

Figure 7 Fiber tensile strength goal for high temperature superalloy composites.

3.2. Fiber quality

Crystal perfection is a strong function of the molten zone, which in turn is very dependent on composition, the height-to-diameter ratio (HTOD, defined in Fig. 5), and the viscosity and surface tension of the melt. Additional processing issues include homogeneity and batch-to-batch variation in the feedrod, diameter variations after the first melt due to density variations in the feedrod, the number of melts, identification and control of a dynamic floating zone, frequency of the laser line scan, unequal laser heating, thermal conductivity of different feedrods, fiber guide placement, growth rate, and chemical analysis difficulty. These issues are manageable for many compositions as optimum conditions are determined for each. Equipment performance, however, has not been linear over time and adjustments are required on a continuing basis.

The summation of all LFZ variables may be largely normalized by observing and controlling the molten zone, quantified by a HTOD ratio. Feedrod composition, density, and diameter are dictating factors for molten zone behavior. For example, increasing levels of yttria increases the viscosity of the melt and allows for greater zone volume. This larger volume is desired in order to assure a totally liquid area and no occurrance of liquid + solid. Multiple melts at attenuation ratios greater than one reduce the volume in the molten area and create more of a potential for liquid + solid, especially if the laser focus is not optimized. Lower viscosity melts are physically more difficult to maintain in a large HTOD molten zone and cause more fluctuations in the fiber diameter. It is believed that the presence of solids in the molten zone is the main cause for run-to-run variability, and also for interfering with seeding. Our experience is that higher values of the HTOD ratio of up to 5 are desired for a fine diameter single crystal fiber. In some cases, however, the viscosity of the melt is such that an HTOD of only 1 is possible without risking separation at the molten area.

It is also important to minimize the number of times the fiber is remelted. It was determined, however, that at least two melts are required to achieve a final crystal diameter on the order of 175 μm. Fiber diameter irregularities are reproduced from melt to melt as they are induced from molten zone volume changes associated with cross-sectional area variation in the feedrod. Another reason to minimize the number of melts is that composition changes could occur during multiple melts due to the disparity between the high-temperature vapor pressures of feedrod components [23]. Fibers are characterized by their starting compositions because no reliable compositional analysis is available at this time. Compositional dependence of the fiber upon remelting is indicated in Table I.

TABLE I Compositional dependence of the fiber upon remelting (mol %)

		ZrO_2	Y_2O_3	HfO_2	Ta_2O_5
ZrO_2-14Y_2O_3-5HfO_2	1st melt	74.5	23.5	2.0	
	2nd melt	79.2	19.5	1.2	
ZrO_2-17Y_2O_3-3Ta_2O_5	1st melt	76.5	19.9		3.6
	2nd melt	76.1	20.2		3.7
	3rd melt	77.1	20.5		2.4

Surface appearance and fiber diameter consistency were also contributing factors in the judgment of fiber quality.

3.3. Fiber selection

ZrO_2 fibers are potential candidates for MMC reinforcement because they possess a higher thermal expansion coefficient than other ceramic fibers. Dissimilar coefficients of thermal expansion (CTE) between the fiber and the matrix creates a potential for internal stresses resulting from severe temperature fluctuations experienced during fabrication or service.

Coefficient of thermal expansion information is presented in Fig. 8 for both binary and ternary fibers based on ZrO_2-Y_2O_3. The highest reported average CTE for ZrO_2 is $\sim 15 \times 10^{-6}/^{\circ}$C at room temperature to 1000°C [25]. The CTE value for these ternaries is slightly lower than this, $\sim 13.5 \times 10^{-6}/^{\circ}$C. The influence of the dopants on CTE was not significant, although a tendency toward decreasing CTE with increasing HfO_2 concentration did exist. The CTE of the Ta_2O_5 containing alloys was slightly higher than that for the HfO_2 or Sc_2O_3. Orientation effects on CTE were not measured on these specimens, however, the CTE values are very close to the literature value for ⟨1 0 0⟩.

The elastic modulus of the ZrO_2-14Y_2O_3-5HfO_2 fibers was correlated with crystal orientation. Based on elasticity theory, the elastic modulus of the cubic crystal system is dependent on crystal orientation [26]. Using exact, measured orientations to properly resolve the applied stress for each tested fiber (i.e. [0.85 0.72 1] instead of [1 1 1]), the direction vector was calculated,

$$R = l_1^2 l_2^2 + l_2^2 l_3^2 + l_3^2 l_1^2$$

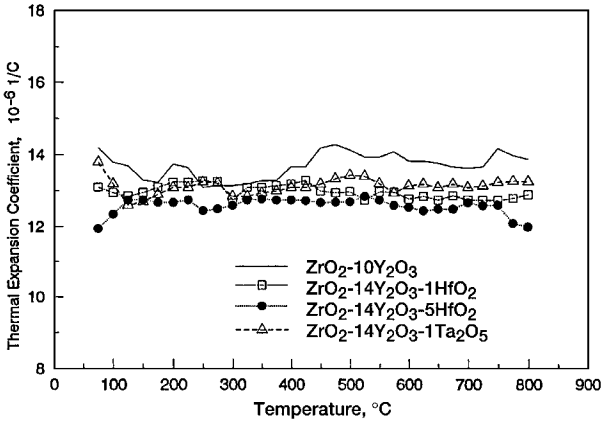

Figure 8 Coefficient of thermal expansion of single crystal ZrO_2 fibers.

TABLE II Measured and calculated Young's Modulus of ZrO_2-14Y_2O_3-5HfO_2 at room temperature (MPa × 10^3)

Orientation	Measured	Calculated
[1 1 1], 8 degrees off [0.85 0.72 1]	219	—
[1 1 1], 8 degrees off [0.85 0.72 1]	238	—
[0 0 1], 3 degrees off [0.09 0.09 1]	394	—
[0 0 1], 3 degrees off [0.09 0.09 1]	359	—
[1 1 0], 13 degrees off [0.63 0.64 1]	306	—
[1 1 0], 17 degrees off [0.53 0.81 1]	359	—
[1 1 0], 11 degrees off [0.61 0.63 1]	345	—
[1 1 1]	—	265
[1 1 0]	—	286
[0 0 1]	—	377

where l_1 is for [1 0 0], l_2 for [0 1 0], and l_3 for [0 0 1] orientations. With the R value included, the stiffness is calculated using [27],

$$1/E = s_{11} - 2 * (s_{11} - s_{12} - s_{44}) * R$$

where s_{11}, s_{12}, and s_{44} are the compliance tensor notations. Table II and Fig. 9 show the measured elastic moduli and those estimated for the optimum orientation. This value was close to the literature [27] for the ⟨1 0 0⟩ orientation. With the ternary system, the difference in the modulus for three different orientations was much smaller than the reference [27] where binary YSZ has been reported to be anisotropic with the highest modulus on ⟨1 0 0⟩. The reason for this was not clear. The relative isotropy of the modulus in the ternary fibers is desirable unless the actual modulus value is less than that of binary partially stabilized zirconia. The result of relative modulus isotropy in ternary compositions suggests that there may be no significant modulus or strength decrease, even if the crystal orientation is slightly off from the desired ⟨1 0 0⟩ orientation.

3.4. Fiber selection

The approach to arrive at a high-expansion and high-strength fiber was first centered around a concept to develop a fiber that included a precipitating second phase for strength improvement. Polycrystalline ZrO_2 can be precipitation hardened for improved strength and creep resistance [10]. Ta_2O_5 was initially thought to be a good ternary candidate based upon a precipitate, Phase V, present in the binary ZrO_2-Ta_2O_5 phase diagram (Fig. 10) at about 5 mol % Ta_2O_5 [28]. Physically, however, the YSZ crystals with ternary Ta_2O_5 additions between 1 and 7 mol % were tough to grow because the molten zone viscosity was too low and the solidus front was not clear. Scanning electron microscopy analysis on grown fibers did not reveal a Phase V in the alloys investigated.

Not all fiber types behave in a similar fashion in floating zone growth. The best approach appears to be to

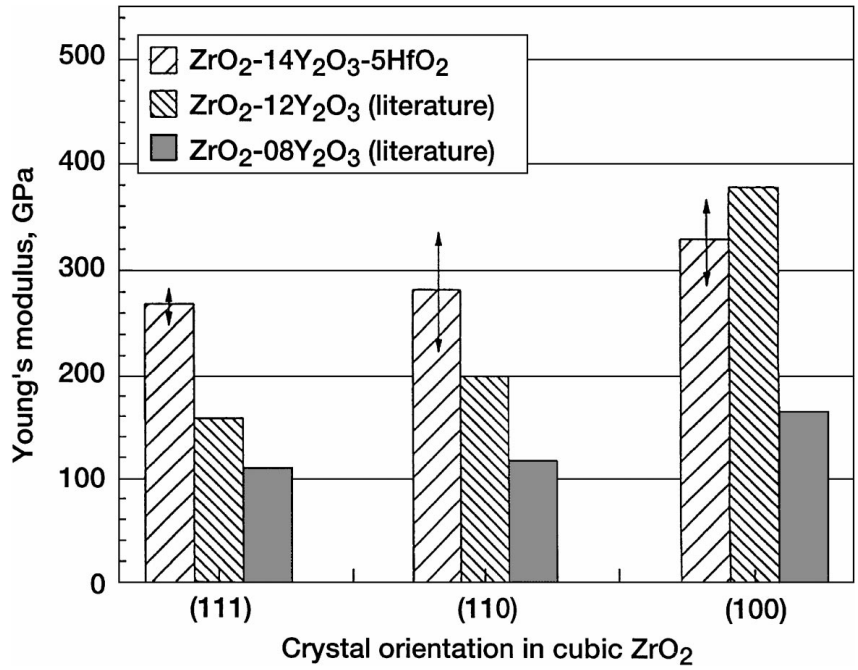

Figure 9 Room temperature Young's modulus comparison for several zirconia-based fibers.

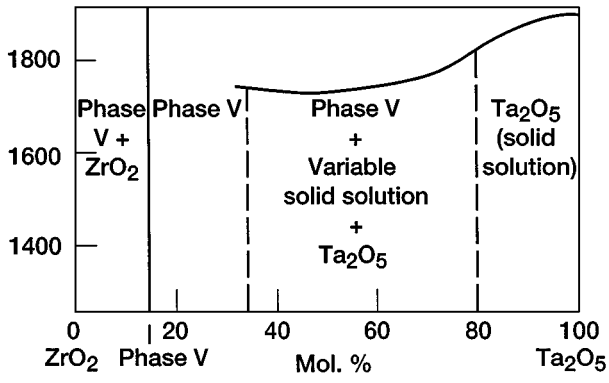

Figure 10 ZrO_2-Ta_2O_5 phase diagram indicating the presence of Phase V.

TABLE III Some physical properties for several candidate oxides

Oxide	Molecular weight	Density (g/cc)	Melting point (°C)
ZrO_2	123.22	5.6	2700
Y_2O_3	225.8	4.84	2410
Ta_2O_5	441.76	8.7	1890
TiO_2	79.9	4.2	1900
La_2O_3	325.82	6.5	2300
HfO_2	210.60	9.7	2800
Cr_2O_3	152.02	5.2	2400
CaO	56.08	3.3	2600
Al_2O_3	101.96	3.65	3630
MgO	40.31	3.57	2784
Sc_2O_3	137.91		2470
Er_2O_3	382.52		3000
Yb_2O_3	394.08		2346

identify a singular fiber composition type and tailor the LFZ process to optimize fiber growth. It was determined that this could be most effectively done in three stages. First, three oxide materials (Ta_2O_5, Sc_2O_3, and HfO_2) were downselected from the group listed in Table III based on growth behavior and attractive physical properties. Steps two and three were arrived at through statistical methods.

The second step, through DOE, selected the most statistically superior and promising (HfO_2) of the three ternary oxide candidates. Significantly more effort would have been required to create three models with accurate predictive capability, therefore, the first design served as only a downselection step. Each of three cases for ZrO_2- [14–24] Y_2O_3- [1–5] X_aO_b (three oxide materials Ta_2O_5, Sc_2O_3, and HfO_2) was investigated. It was determined that 5 mol % X_aO_b would be the maximum ternary addition due to density considerations (Table III). A full-factorial design was employed for each ternary system so that each design could stand alone and be analyzed independently. The negative effect to such an approach is a limited amount of data at each point for accurate modeling. To improve upon this, replicates

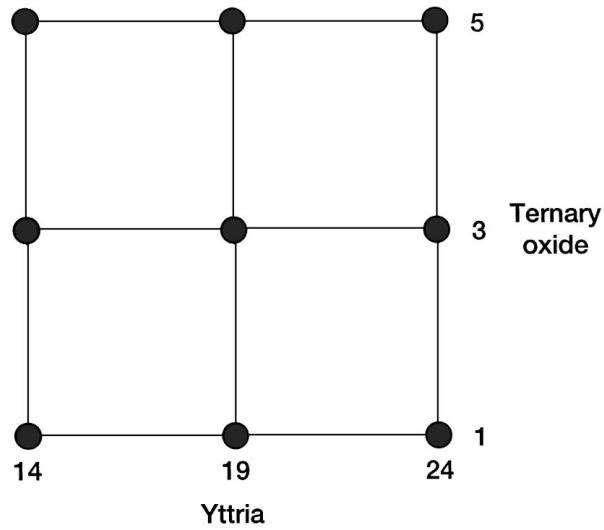

Figure 11 Design space for ZrO_2-Y_2O_3-X_aO_b investigation.

(defined as data obtained from fibers grown from separate feedrods) at each condition in Fig. 11 would be necessary. In the data presented below, replicates were

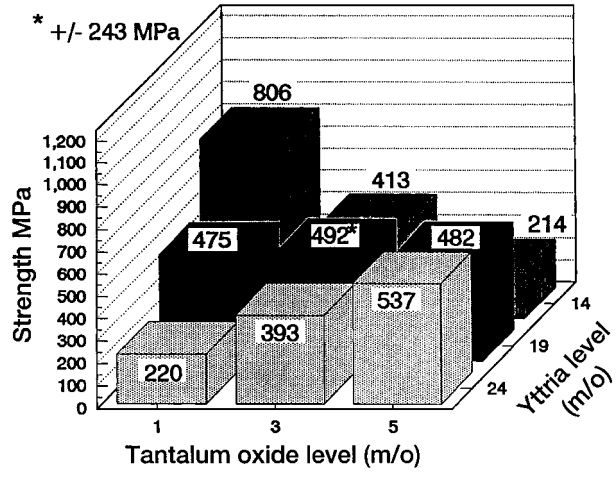

(a)

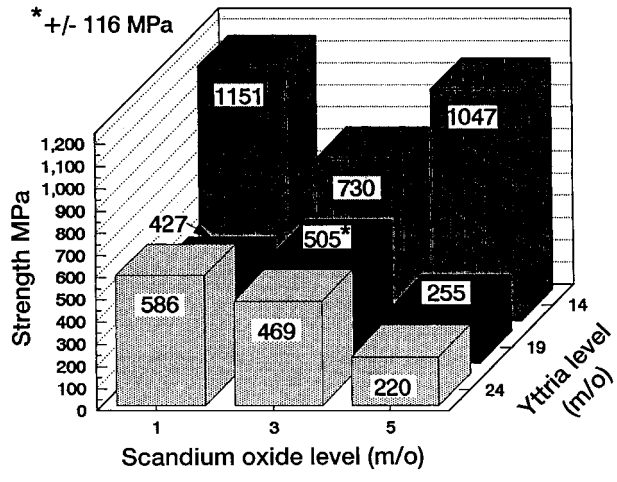

(b)

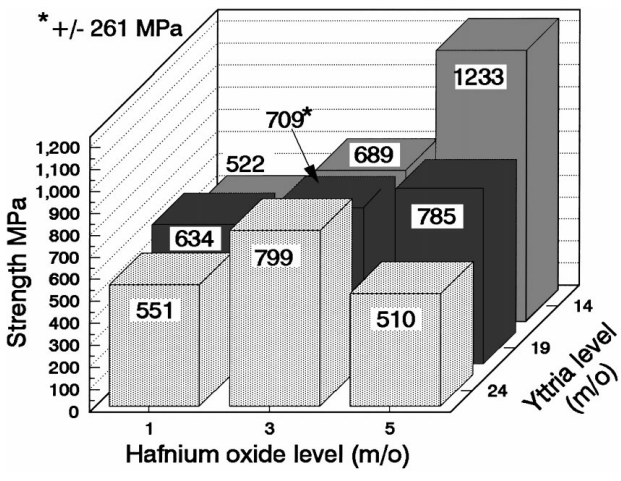

(c)

Figure 12 Raw data plot for ternary oxide (a) Ta_2O_5, (b) Sc_2O_3 and (c) HfO_2.

performed only at the centerpoint of each design and each of the other strength values represent an average of at least four tests within the one batch.

The high temperature strength values of the fibers from step one DOE are seen in Fig. 12. Fibers deformed and failed without measurable plasticity, with most failing inside the furnace hot zone. Figs 12a, b, and c show the 816 °C tensile results for $X_aO_b = Ta_2O_5$, Sc_2O_3, and HfO_2. Included on each figure is a plane at 700 MPa which indicates the goal strength for ZrO_2-based fiber at $V_f = 0.4$. A fiber which consistently performs above this level would contribute to composite performance that is equal to or exceeds the goals that were set in Fig. 7. Standard deviations are only given for the centerpoints of each design (ZrO_2-$19Y_2O_3$-$3X_aO_b$) because that was the only composition that was replicated to examine batch-to-batch variation. Specifically, three different batches of feedrod were processed and analyzed separately at the center of the design as opposed to only one batch investigated at each of the other conditions. Each of the other strength values presented on the figures represent an average of multiple tests but were assigned as a single value by defining them as a single batch. The variation within a batch is dependent upon the composition (i.e. for ZrO_2-$14Y_2O_3$-$5HfO_2$ the standard deviation is ±275 MPa). The large standard deviations at the centerpoints with respect to the mean strength value could indicate that batch-to-batch consistency is difficult to achieve. This, however, is complicated by the fact that the ease of fiber growth and fiber quality are such strong functions of composition. This will be discussed later in the fully replicated statistical methods analysis of $X_aO_b = HfO_2$ where it was found that standard deviations were not consistent across the design space when replications at each point were included. At ZrO_2-$19Y_2O_3$-$3X_aO_b$ in Figs 12a–c the standard deviations range from 20% to 50% of the mean strength values.

In both cases of Sc_2O_3 and HfO_2 ternary addition molten zone viscosities were noticeably higher than that of Ta_2O_5, and these compositions were easier to grow than those that included Ta_2O_5. Fig. 13 summarizes the fiber growth behavior from the molten zone as a function of the ternary composition, indicating the composition range where crystals were grown successfully.

In determining the most promising X_aO_b, Ta_2O_5 is quickly eliminated from contention for further study based on low 816 °C tensile values. The raw data are pictorially shown in Fig. 12a and visually compared to Figs 12b and c. Even the most promising combinations at low Y_2O_3 and Ta_2O_5 levels in Fig. 12a are not

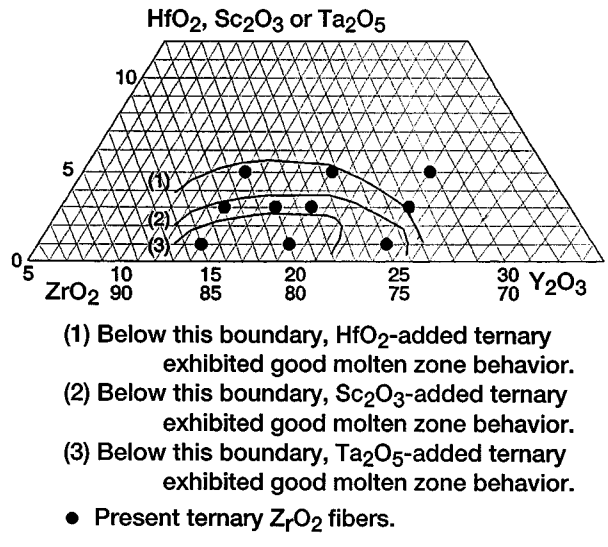

Figure 13 Fiber growth feasibility in ternary space.

high enough to consistently exceed the strength goals of 700 MPa. Physically, compositions of $X_aO_b = Ta_2O_5$ were difficult to grow which translates into inconsistent fiber quality, and is reflected in the large standard deviation at the centerpoint equal to 50% of the mean strength value. Statistically, it was determined that, on the average, compositions including 1 to 5 mol % Ta_2O_5 were significantly lower than those compositions including Sc_2O_3 and HfO_2 (at a 95% confidence level). It appears that the anticipated benefit of Phase V was absent in the ternary space examined.

The strength results for Sc_2O_3 and HfO_2 in Fig. 12b and c indicate that while both ternary compounds produced compositions with very high strengths, HfO_2 results were more consistently higher across the design space. With 95% confidence, the average strengths of all the compositions containing HfO_2 are marginally statistically higher than compositions containing Sc_2O_3. This statement validates what may be inferred from inspection of the two raw data plots in Figs 12b and c where it appears that HfO_2 results are consistently higher across the design space and closer to the goal plane at 700 MPa. It is clear in both figures that the greatest strength potential is achieved at lower yttria levels. Before making a final choice as to which X_aO_b would be chosen for comprehensive investigation, two additional, separate fiber batches were prepared at ZrO_2-$14Y_2O_3$-1 X_aO_b and ZrO_2-$14Y_2O_3$-5 X_aO_b where $X_aO_b = Ta_2O_5$, Sc_2O_3, and HfO_2. These results may be used as verification of the presented data in Fig. 12 and show batch-to-batch variation at those compositions. Table IV summarizes these results.

The most significant result of these verification experiments is at $X_aO_b = Sc_2O_3$ and their comparison to Fig. 12b. It is obvious from Fig. 12b that the lower yttria compositions were the most promising, but the strength values appeared to be unrealistically sensitive to very small ternary additions. Specifically, 816 °C tensile strengths going from 1151 MPa down to 730 MPa and then back up to 1047 MPa as Sc_2O_3 ranges from 1 to 5 mole percent is unlikely to be real. The verification experiments (batches 2 and 3) could not reproduce the high strength values in batch 1, and this resulted in eliminating Sc_2O_3 from further consideration.

The HfO_2 results in Table IV in comparison with Fig. 12c were more hopeful and indicated that the repeat batches 2 and 3 consistently gave strengths above the 700 MPa goal at both solute levels. Thus, ternary oxide type HfO_2 was identified as the choice for detailed investigation as an addition to yttria-stabilized zirconia.

Upon choosing $X_aO_b = HfO_2$ as the promising ternary component to ZrO_2-Y_2O_3-X_aO_b for MMC application, a more exhaustive full-factorial DOE design determined the most favorable composition (ZrO_2-$14Y_2O_3$-$5HfO_2$) for the chosen ternary system. The experiments were fully replicated. The repeat experiments were valid replicate experiments as they were from different batches of fibers and batch-to-batch variation was considered in the analysis. Data is shown in Table V.

Visual examination of the data suggested that the standard deviations were not the same across the design space, therefore the standard deviation was modeled to inspect this. The statistical analysis corroborated the visual suspicion. Therefore, the mean tensile strength had to be modeled using the weighted linear least squares regression technique [29] (weight = 1/(standard deviation)^2). The disadvantage of this approach is that points without replication had to be excluded from the fit since they had no standard deviation and therefore no estimated weights. These values were instead used as confirming experiments.

Model predictions for strength were able to be made with 95% confidence. Table VI provides 95% confidence predictions at the levels indicated in Fig. 14. The

TABLE V Strength results and modeled data for specific fiber chemistry combinations in the ZrO_2-Y_2O_3-HfO_2 system

Yttria level	Hafnium oxide level	Fiber strength (MPa)	Modeled standard deviation
14	1	496	250
14	1	648	250
14	1	985	250
14	5	1233	194
14	5	992	194
14	5	847	194
19	3	365	218
19	3	765	218
19	3	703	218
19	3	372	218
19	3	813	218
24	1	551	14
24	1	579	14
24	1	558	14
24	5	510	100
24	5	696	100
24	5	537	100
14	3	689*	N/A
19	1	634*	N/A
19	5	785*	N/A
24	3	799*	N/A

*Confirming experiments.

TABLE VI Model predictions for ZrO_2-Y_2O_3-HfO_2 system

Mol %	$Y_2O_3 = 14$	$Y_2O_3 = 19$	$Y_2O_3 = 24$
$HfO_2 = 1$	659 ± 504 MPa	610 ± 273 MPa	562 ± 124 MPa
$HfO_2 = 3$	826 ± 321 MPa	697 ± 198 MPa	568 ± 159 MPa
$HfO_2 = 5$	994 ± 408 MPa	783 ± 248 MPa	573 ± 238 MPa

TABLE IV Batch-to-batch strength variation within different oxide types *ZrO_2-$14Y_2O_3$- [1, 5] X_aO_b multiple tests were performed in each batch

	Ta_2O_5 (MPa)			Sc_2O_3 (MPa)			HfO_2 (MPa)		
X_aO_b level (mol %)*	batch 1	batch 2	batch 3	batch 1	batch 2	batch 3	batch 1	batch 2	batch 3
1	806	448	758	1151	813	806	496	648	985
5	214	131	475	1047	682	675	1233	992	847

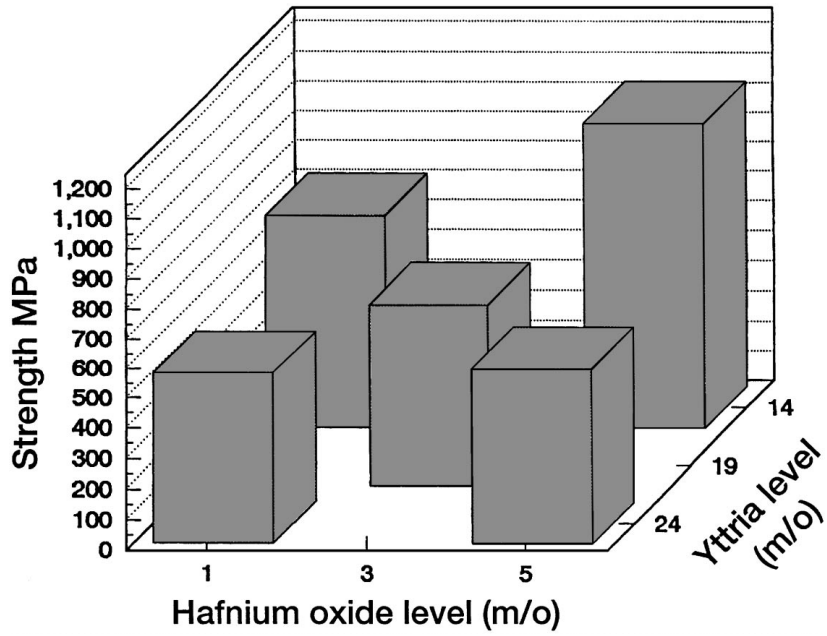

Figure 14 Strength results of fully replicated design of experiment for ternary oxide HfO_2.

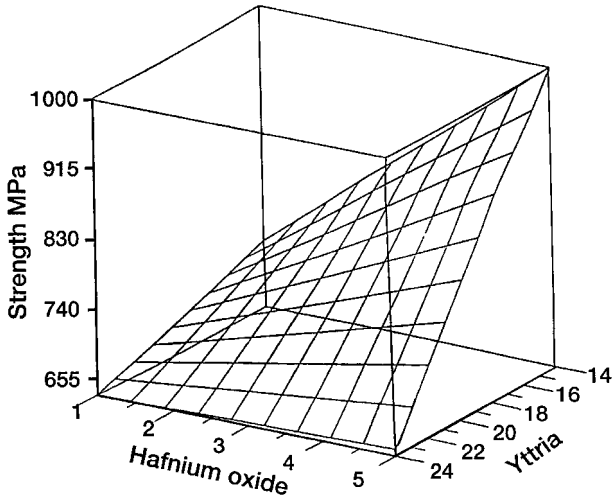

Figure 15 Three-dimensional response surface predicting X_aO_b-HfO_2 ternary behavior.

fully replicated experiments in Fig. 14 yielded reliable, yet modest, results. These results represent three separate batches of fibers at each composition. The obvious conclusion here is that the only condition that exceeds the goal of 700 MPa and has a chance of consistently exceeding it is at $81ZrO_2$-$14Y_2O_3$-$5HfO_2$. Fig. 15 is the graphical response surface for the modeled analysis.

The confirming experiments from Table V are within the confidence bands shown in Table VI, except at the yttria = 24, hafnium oxide = 3 level. The small nature of the error bars at this point are due to its close proximity to the yttria = 24, hafnium oxide = 1 level where the repeats may have been unusually close to each other (i.e. 579, 551, 558 MPa). The variation in 95% confidence intervals from composition to composition as seen in Table VI is apparently related to both composition and processing difficulty.

Optimization of the LFZ generated fiber system ZrO_2-Y_2O_3-HfO_2 can be visually conducted by simply looking at the three-dimensional graph in Fig. 15. To maximize strength, $81ZrO_2$-$14Y_2O_3$-$5HfO_2$ should be used. Table VI indicates this also and predicts with 95% confidence (~2 standard deviations) that strength is 994 ± 408 MPa. This predicted performance is above but very close to the fiber strength goal.

The resultant model for the compositional effect on 816 °C tensile strength (Fig. 15) showed a significant effect due to yttria level and marginally significant effects due to hafnium oxide level and yttria/hafnium oxide interaction. The equation for the 816 °C tensile strength is

$$\sigma_i = 101.13 - 18.73X_1 + 12.52X_2 - 11.73X_1X_2$$

where X_1 = yttria level (mol %) and X_2 = hafnium oxide level (mol %). Caution should be exercised when referring to the modeled equation above because of batch-to-batch variation and the large 95% confidence intervals indicated in Table VI.

3.5. Fiber orientation effect

Success in seeding depends primarily on focusing of opposite beams. The interface must not only be flat, but both sides must be molten. If an unequal heating condition exists in the molten area and one side is liquid + solid, then seeding will be compromised. Floating zone conditions must remain optimized throughout the seeding and fiber growth procedure. If careful control is not taken, fiber orientation tends to drift. It should also be added that cubic zirconia materials have been difficult to seed and maintain desired orientations [30]. During one experiment in the present study, a fiber with a ⟨0 0 1⟩ orientation for $81ZrO_2$-$14Y_2O_3$-$5HfO_2$ was successfully seeded and grown, maintaining its preferred orientation along its 250 mm length. This experiment, unfortunately, was difficult to reproduce with any regularity and therefore no definite conclusions or assumptions

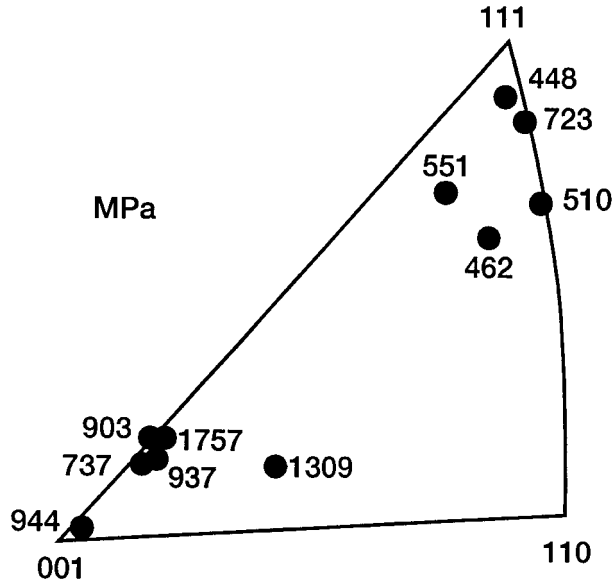

Figure 16 Orientation dependence of ZrO_2-$14Y_2O_3$-$5HfO_2$ single crystal fiber.

are made with respect to the orientation contribution of these fibers to strength behavior.

The inability to seed these fibers is unfortunate, and this study therefore contained ranges of crystal orientation. The strength results and their correlation to the standard triangle are, in most cases, uninteresting. Fibers of compositions covering the full design space indicated in Fig. 11 for $X_aO_b = Ta_2O_5$, Sc_2O_3, and HfO_2 were investigated. Multiple orientations in each case were examined for an orientation effect on strength. However, except for the data shown in Fig. 16, strength and orientation combinations were random across the standard triangles indicating no correlation. Instead, strength values appeared to be more determined by flaws in the crystals. Considering Fig. 16, it seems that an argument could be made for fiber composition $81ZrO_2$-$14Y_2O_3$-$5HfO_2$ with regard to its strength dependence on orientation. Fig. 16 hints that a $81ZrO_2$-$14Y_2O_3$-$5HfO_2$ fiber with near ⟨0 0 1⟩ orientation (1096 ± 372 MPa) is superior to the same fiber with near ⟨1 1 1⟩ orientation (537 ± 110 MPa). Statistically, based on a 1n-transformed Aspin-Welch *t*-test [31] we can state with 99.8% confidence that the means of these two populations are different. Type ⟨1 1 0⟩ fibers were not included because they were difficult to grow. Assuming that a case could be made for strength dependence on orientation in the $81ZrO_2$-$14Y_2O_3$-$5HfO_2$ fiber, seeding procedures are not fully reproducible at this time and fibers of preferred orientation cannot be reliably grown. This, unfortunately, was the case for all compositions grown, forcing the comparison of average properties without an orientation effect to arrive at conclusions.

4. Conclusions

The development of fibers for reinforcement in high-temperature MMCs is a formidable task. In order to be considered, fibers must include most of the following factors – high temperature strength and creep resistance, low density, high modulus, a CTE that is close to that of the matrix, chemical compatibility with the matrix, and specific stiffness.

Fibers with compositions based on zirconia have melting temperatures approaching 3000 °C. The LFZ apparatus is a likely choice to investigate such fibers as it is capable of producing high melting temperature fibers in experimental lengths since no crucible is needed. An alternative fiber growth method would have to be developed for production scale-up.

Statistical methods were used to analyze the fast fracture tensile strength of fibers and it was found that the HfO_2-added ternary was superior to the Ta_2O_5 and Sc_2O_3 additions and the higher HfO_2 additions were more effective at lower Y_2O_3 content (i.e. $14Y_2O_3$-$5HfO_2$). An optimum ternary fiber composition based on yttria-stabilized zirconia was chosen based on its tensile strength behavior at 816 °C. It can be stated statistically with 95% confidence that ZrO_2-$14Y_2O_3$-$5HfO_2$ fiber strength is 992 ± 407 MPa at 816 °C. In other words, 95% of the tests performed will have strengths in that range. This includes the assumption that the effect of orientation is neglected and we are just comparing average properties. This result implies that a composite with this fiber and an appropriate matrix would be competitive with nickel-base superalloy strength performance at 816 °C. The complexity of the LFZ apparatus and the batch-to-batch variability would require improvement.

There are still, however, many unanswered composite issues. Fiber degradation, chemical reaction, the high density of the fiber material, high-temperature modulus, thermal stability, creep resistance, and thermomechanical responses still require attention.

Acknowledgements

The authors would like to acknowledge Mr. Dennis Keller of RealWorld Quality Systems Incorporated for the statistical design and statistical interpretation contained in this work.

References

1. J. A. DICARLO and S. DUTTA, in "Handbook on Continuous Fiber Reinforced Ceramic Matrix Composites," edited by R. Lehman, S. El-Rahaiby, and J. Wachtman, Jr. (Purdue University, West Lafayette, Indiana, 1995) p. 137.
2. F. J. RITZERT and L. WESTFALL, NASA TM 4732, January 1996.
3. W. B. PERRY and R. C. VENTURA, in Proceedings of HITEMP Review 1993, Vol. 3 (NASA Conference Publication 19117, 1993) p. 82–91.
4. S. L. DRAPER and I. E. LOCCI, *J. Mater. Res.* **9** (1994) 1397.
5. J. A. DICARLO, J. B. HURST, G. N. MORSCHER, A. SAYIR and G. SELOVER, in Proceedings of HITEMP Review 1990 (NASA Conference Publication 10051, 1990) p. 50–61.
6. R. L. CRANE and R. E. TRESSLER, *J. Comp. Mater.* **5** (1971) 537.
7. G. S. CORMAN, Air Force Report WRDC-TR-90-4059, 1990.
8. P. E. HEYDT, A. SAYIR and R. E. TRESSLER, *Ceramic Trans.* **74** (1996) 37.
9. L. WESTFALL and F. RITZERT, in Proceedings of HITEMP Review 1994. Vol. 3 (NASA Conference Publication 19146, 1994), p. 72–81.

10. J. MARTINEZ-FERNANDEZ, M. JIMENEZ-MELENDO, A. DOMINGUEZ-RODRIGUEZ and A. H. HEUER, *J. Amer. Ceram. Soc.* **73** (1990) 2452.
11. K. J. MCCLELLAN, H. SAYIR, A. H. HEUER, A. SAYIR, J. HAGGERTY and J. SIGALOVSKY, *Ceram. Eng. Sci. Proc.* **14** (1993) 651.
12. G. N. MORSCHER, P. PIROUZ and A. H. HEUER, *J. Amer. Ceram. Soc.* **74** (1991) 491.
13. A. DOMINGUEZ-RODRIGUEZ, K. P. D. LAGERLOF and A. H. HEUER *ibid.* **69** (1986) 281.
14. H. G. SCOTT, *J. Mater. Sci.* **10** (1975) 1527.
15. D. J. KELLER, "Introduction to Design of Experiments, Theory-Methods-Applications" (Real World Quality Systems, Inc., Rocky River, OH, 1993) p. 343.
16. W. E. LEE and W. M. RAINFORTH, "Ceramic Microstructures, Property Control by Processing" (Chapman & Hall, London, 1994) p. 10.
17. L. WESTFALL, private communication, 1994.
18. D-3379-75: ASTM Standard Test Method for Tensile Strength and Young's Modulus for High Modulus Single Filament Materials, ASTM Committee D-30, 1975.
19. D. J. PYSHER, Creep rupture behavior of alumina-based ceramic fibers, PhD thesis, Pennsylvania State University, State College, PA, 1992.
20. J. C. GOLDSBY, private communication, 1995.
21. Mettler TA 4000: Operating Instructions, Mettler Instrument Corp., P.O. Box 71, Hightstown, NJ 08520-0071.
22. J. C. GOLDSBY, H. M. YUN and G. N. MORSCHER, in Proceedings of HITEMP Review 1993, Vol. 3 (NASA Conference Publication 19117, 1993) p. 85–91.
23. D. G. HARLOW and S. L. PHOENIX, *J. Comp. Mater.* **12** (1978) 195.
24. W. B. HILLIG, in "Tailoring Multiphase and Composite Ceramics," edited by R. E. Tressler, G. L. Messing, C. G. Pantano and R. E. Newham (Plenum, New York, 1986) p. 697.
25. Y. S. TOULOUKIAN, R. K. KIRBY, R. E. TAYLOR and T. Y. R. LEE, in "Thermal Expansion Nonmetallic Solids" (IFI/Plenum, New York, 1975) p. 451.
26. J. F. NYE, "Physical Properties of Crystals" (Oxford University Press, 1979) p. 144.
27. R. P. INGEL, D. LEWIS, B. A. BENDER and R. W. RICE, in "Advances in Ceramics, Science and Technology of Zirconia II," edited by N. Claussen, M. Ruehle, and A. H. Heuer (American Ceramic Society, 1984) p. 408.
28. E. M. LEVIN, C. R. ROBBINS and H. F. MCMURDIE, "Phase Diagrams for Ceramists" (The American Ceramic Society, Columbus, OH, 1964) p. 144.
29. D. J. KELLER, "Advanced DOE, Regression, and Optimization" (Real World Quality Systems, Inc., Rocky River, OH, 1993) p. 603.
30. L. W. WESTFALL, private communication, 1995.
31. A. HALD, "Statistical Theory With Engineering Applications" (John Wiley & Sons, New York, 1965) p. 394.

Received 15 September
and accepted 15 September 1998